Exp Oncol 2018
40, 1, 24–32

Experimental ONCOLOGY

IMPACT OF ENDOSTATIN GENE THERAPY ON MYELOID-DERIVED SUPPRESSOR CELLS FROM A METASTATIC RENAL CELL CARCINOMA

*K.C.B. Chaves[1], E.M. Costa[2], L.F. Teixeira[2], M.H. Bellini[1, 2, *]*
[1]*Department of Medicine, Nephrology Division, Federal University of São Paulo, São Paulo 04039-000, Brazil*
[2]*Biotechnology Department, Nuclear and Energy Research Institute, São Paulo 05508-000, Brazil*

Aim: **To evaluate the role of endostatin (ES) gene therapy on myeloid-derived suppressor cells (MDSC) in a metastatic model of renal cell carcinoma (RCC).** ***Materials and Methods:*** **Balb/C mice bearing orthotopic Renca tumors were treated with NIH/3T3-LendSN or, as a control, with NIH/3T3-LXSN cells. At the end of *in vivo* experiment, plasma and tissue lung samples were collected. Plasma ES and granulocyte colony stimulating factor (G-CSF) levels were measured by ELISA and Milliplex, respectively. Quantification of $CD11b^+Gr\text{-}1^+$ cells and their subsets was performed by flow cytometry. Reactive oxygen species (ROS) production was measured in $CD11b^+Gr\text{-}1^+$ MDSC using the DCFDA marker by flow cytometry.** ***Results:*** **Metastatic RCC (mRCC) induced expansions of $CD11b^+Gr\text{-}1^+$ MDSC and promoted accumulation of these cells and their subtypes in lymphoid organ and metastases. ES treatment promoted low G-CSF plasmatic levels which were produced by the tumor microenvironment, reflecting the reduced metastatic accumulation of $CD11b^+Gr\text{-}1^+$ MDSC in the lungs. However, the therapy was selective for granulocytic cells, thus reducing the production of ROS.** ***Conclusion:*** **These findings confirm the expansion of MDSC during metastatic progression of RCC and indicate the important role of ES in reducing MDSC and possible use of ES therapy in combined anticancer treatment.**
Key Words**: renal cell carcinoma, endostatin, gene therapy, myeloid-derived suppressor cells.**

Renal cell carcinoma (RCC) is the most common neoplasm in the kidney [1]. The incidence of RCC has significantly increased over the past several years, mainly in North America and in the majority of Europe [2]. The American Cancer Society estimates at least 62,700 new cases and approximately 4,240 deaths in the United States for 2016 [1].

It is estimated that more than 30% of patients with RCC have metastatic disease at the time of diagnosis [3]. On the other hand, if diagnosed early, RCC is associated with a favorable prognosis of ~85% of a 5-year survival rate [4].

The most common histologic subtype of RCC is clear cell renal cell carcinoma (ccRCC), which represents 75% of parenchymal tumors. Moreover, some chromosomal abnormalities have been documented in ccRCC, including von Hippel — Lindau (VHL) mutations on 3p25-26, 3p14.2 and 3p12 [5, 6]. In the majority of hereditary ccRCC tumors and in up to 92% of sporadic ccRCC tumors are associated with VHL gene defects in which the gene is inactivated [7]. The aggressive behavior of ccRCC is related to a VHL gene mutation that leads to stabilization of hypoxia-inducible factors (HIF-1α and HIF-2α) that in turn upregulates hypoxia-response genes, including vascular endothelial growth factor (VEGF) [8].

The tumor microenvironment, composed of parenchymal and stromal compartments, may release growth factors and cytokines to induce an immunosuppressive response [9]. These molecules contribute to the rapid recruitment, expansion and activation of several immunosuppressive cells, such as regulatory T cells (Tregs), tumor-associated macrophages (TAMs), type 2 natural killer T (NKT) cells, Tie2-expressing monocytes, N2 neutrophils and myeloid-derived suppressor cells (MDSC) [10]. Studies have correlated an increased number of MDSC in tumors with poor prognostic outcomes in patients with cancer. Although MDSC are one of the major contributors of tumor-induced immunosuppression, they actively participate in tumorigenic activities. These cells produce angiogenic factors, such as VEGF, basic fibroblast growth factor (bFGF), HIF-1, tumor growth factor beta (TGF-β) and matrix metalloprotease (MMP)-9, which are able to alter the environment to a pre-metastatic profile and promote neoangiogenesis [11].

MDSC are a major component of the immune suppressive network. In healthy individuals, immature myeloid cells (IMC) differentiate into macrophages, granulocytic and dendritic cells in bone marrow. In contrast, under various pathological conditions, such as cancer, a partial block of the differentiation of IMC leads to their expansion. These expanded IMC under pathological conditions are termed MDSC because of their immune suppressive properties. MDSC are composed by progenitor cells and IMC, which are identified in mice using the CD11b and Gr-1 markers [12–14].

Submitted: January 31, 2018.
*Correspondence: E-mail: mhmarumo@terra.com.br
Abbreviations used: bFGF – basic fibroblast growth factor; ccRCC – clear cell renal cell carcinoma; ES – endostatin; G-CSF – granulocyte colony stimulating factor; HIF – hypoxia-inducible factors; IMC – immature myeloid cells; MDSC – myeloid-derived suppressor cells; MMP – matrix metalloprotease; mRCC – metastatic RCC; NKT – type 2 natural killer T cells; RCC – renal cell carcinoma; ROS – reactive oxygen species; TAMs – tumor-associated macrophages; TGF-β – tumor growth factor beta; Tregs – regulatory T cells; VEGF – vascular endothelial growth factor; VHL – von Hippel – Lindau.

Notably, in cancer, MDSC are distributed among the primary and secondary lymphoid organs and the tumor site. Numerous tumor-secreted factors, including cyclooxygenase 2, prostaglandins, stem-cell factor (SCF), monocyte-colony stimulate factor (M-CSF), interleukin-6 (IL-6), granulocyte/macrophage-colony stimulating factor (GM-CSF) and VEGF are known to induce MDSC expansion and modify the myelopoiesis process. Furthermore, most of these factors can trigger signaling pathways involving Janus kinase (JAK) protein family members and signal transducer and activator of transcription 3 (STAT3) in MDSC, promoting cell survival, proliferation, reduced apoptosis and the prevention of the differentiation of myeloid progenitors into mature cells [10, 12].

However, two subsets have been identified within MDSC, namely granulocytic (G) or polymorphonuclear (PMN)-MDSC and monocytic or mononuclear (M)-MDSC. Based on the analyses of different tumor experimental models, PMN-MDSC are the most predominant, representing at least 70–80% of MDSC. In addition, MDSC subsets distinctly induce suppressive mechanisms. The PMN-MDSC subset produces high levels of reactive oxygen and nitrogen species (ROS and RNS) and myeloperoxidase. In addition, peroxynitrite, a reactive nitrogen species, was also reported to be produced by PMN-MDSC. PMN-MDSC suppress T-cell proliferation via a contact-dependent and antigen-specific manner. This mechanism induces nitrosylation or nitration of cysteine, methionine, tryptophan and primarily tyrosine that are present in T cell receptor (TCR)-CD8 complexes [15].

In contrast, M-MDSC trigger suppressive responses by producing high levels of inducible nitric oxide synthase (iNOS) and arginase 1 (Arg1). Both enzymes regulate the bioavailability of the amino acid L-arginine, which leads to a decrease in the CD3ζ-chain, the production of interferon gamma (IFNγ) and interleukin-2 (IL-2) and an inhibition of T cell proliferation. These suppressive effects are mediated in an antigen-nonspecific manner [15, 16].

Therefore, strategies to target MDSC have led to new alternatives for improving antitumor therapies, including the deactivation or depletion of MDSC and their differentiation into mature myeloid cells. Nevertheless, a better understanding of the mechanism of MDSC expansion and activity may provide valuable information for future drug design.

Endostatin (ES) is a 20-KDa C-terminal fragment derived from collagen XVIII that was first purified from murine hemangioendothelioma and observed to exert *in vivo* and *in vitro* anti-tumor and antiangiogenic activities [17]. The mechanisms involved in ES function have not been elucidated. Studies have described molecules of low or high-affinity that bind to ES, such as α_5- and α_v-integrins, glycopican-1 and glycopican-4 [18]. However, ES inhibits MMP-2 and promotes a blockade of VEGF/VEGFR signaling. Moreover, a genomic array analysis of human dermal microvascular endothelial cells after treatment with human recombinant ES showed its involvement in the downregulation of various genes associated with adhesion and matrix degradation, coagulation, apoptosis, angiogenesis and cell-cycle transition [19]. This protein was approved by the State Food Drug Administration (FDA) for the treatment of patients with non-small-cell lung cancer in China. Clinical trials have shown ES to be most effective when combined with other therapies, especially with chemotherapies [20]. This combination is believed to enhance its therapeutic efficacy and reduce side effects.

Recent studies have demonstrated that the use of chemotherapeutic drugs and antiangiogenic tyrosine kinase inhibitors lead to important biological effects in MDSC [21, 22].

In previous reports from our group, the antitumoral effects of ES resulted in an increase in survival rate and reductions in metastatic nodules and tumor area. However, a proinflammatory effect was confirmed based on the recruitment of effector cells to metastatic and secondary lymphoid sites and clonal expansion. Therefore, the efficacy of ES in this model has been shown to abrogate M2 expansion, favoring tumor elimination.

In this study, we evaluated the profile of myeloid cells in a metastatic renal cell carcinoma (mRCC) model and the ES effect on MDSC present in mRCC.

MATERIALS AND METHODS

Cell lines. Renca tumor cells were derived from a murine transplantable renal adenocarcinoma of spontaneous origin obtained from Cell Lines Service (Eppelheim, DEU). These cells were maintained in RPMI 1640 medium from Life Technologies Corporation (Grand Island, NY, USA) supplemented with 10% fetal bovine serum, 2 mM L-glutamine, 1 mM sodium pyruvate, 1% minimal Eagle's medium nonessential amino acids, 100 U/ml penicillin, 100 µg/ml streptomycin and 10% fetal bovine serum from Gibco-Invitrogen (Carlsbad, CA, USA).

NIH/3T3-LendSN-clone 5 and NIH 3T3-LXSN were used for ES expression and controls, respectively, as described previously [23]. Both cell lines were maintained with high-glucose-content (4.5 g/l at 25 mM) Dulbecco's modified Eagle's medium (DMEM) (Life Technologies Corporation) supplemented with 100 U/ml penicillin, 100 µg/ml streptomycin and 10% fetal bovine serum (Gibco-Invitrogen, Carlsbad, CA, USA).

All cell lines were maintained in a humid chamber at 37 °C and under 5% carbon dioxide.

Animals. Thirty male Balb/c mice, aged 8–10 weeks, were obtained from the Animal Facility of IPEN/CNEN-SP, São Paulo, Brazil. All animals were cared for in accordance with the standards of the Institute under a protocol approved by the Animal Experimentation Ethics Committee (Number of process: CEP 105/12).

Orthotopic mRCC model. Mice were anesthetized via intraperitoneal injection of ketamine

(100 mg/kg body weight, Ketalar; Parke-Davis, Morris Plains, NJ, USA) and xylazine (10 mg/kg body weight, Phoenix Scientific, Inc., St. Joseph, MO, USA). Renca cells ($2 \cdot 10^5$) were inoculated into the renal subcapsular space, as previously described [23].

Seven days after Renca cell inoculation, the left kidney was removed via unilateral nephrectomy. The mice were divided into three groups (10 mice/group): control, metastasis and ES-treated.

Metastasis. At the end of experiment, all mice were exsanguinated and euthanized in accordance with the local institutional guidelines for animal care and approved by the University ethics committee. Healthy mice were used as organs and plasma donors for the normal group. The lungs from the group were excised and processed for analysis by flow cytometry.

ES gene therapy. On the day of nephrectomy, the control and ES-treated groups received subcutaneous injections of 3.6×10^6 NIH/3T3-LXSN and NIH/3T3-LendSN-clone 5, respectively. After ten days, the lungs from the control and ES-treated groups were excised and processed for analysis by flow cytometry *in vitro*. A small pulmonary fragment was separated for fixing in methacarn for 3 h (containing 60% methanol, 30% chloroform and 10% glacial acetic acid) for hematoxylin and eosin (HE) staining.

Histological analysis. Methacarn-fixed lungs were processed for paraffin embedding. Histological analysis was performed using 4-µm sections stained with HE, which were analyzed under a light microscope. The images were obtained using a microscope (Leica DM1000, Leica Microsystems, Wetzlar, DEU), a digital compact camera (Leica DFC420C, Leica Microsystems) and an image processor (Leica Application Suite v3.3.0). The quantification of metastatic lesions present in the pulmonary fragment was performed by counting the lesions under a light microscope at a 40x magnification.

Plasma ES levels were measured using a Mouse Endostatin ELISA Kit (Novateinbio® — Accelerates Research and Development — USA) according to the manufacturer's instructions. The ES concentrations were determined at least in duplicate, and the assay reproducibility was confirmed. ELISA plates were read using the Multiskan EX Microplate Reader (Labsystems, Milford, MA, USA*)* Plasma G-CSF levels were determined using the Milliplex (Mouse Cytokine Magnetic Bead Panel, Millipore, Darmstadt, Germany), according to the manufacturer's instructions. The reading was made using a Luminex xMAP 100 system (Luminex Cooperation, Austin, Texas, USA), and the data were processed at the Xponent Software. The data were expressed as the mean fluorescence intensity (MIF).

Preparation of single-cell suspensions. Lungs were cut into smaller fragments (< 1 mm^3) with sterile scissors, transferred to a beaker containing collagenase D at 2.5 mg/ml (Roche Diagnostics, Mannheim, DEU) diluted in RPMI 1640 and incubated for 30 min in a humid chamber at 37 °C under continuous agitation. Next, 2 volumes of phosphate buffer saline (PBS) containing 0.5% fetal bovine serum and 0.5% EDTA at 0.5 M) were added, and then the cell suspensions were filtered through a 70-µm cell strainer (BD Bioscience, San Jose, CA, USA). The tubes were centrifuged at 1500 rpm for 5 min, red blood cells were lysed using ammonium chloride lysis buffer (containing 0.155 M NH_4Cl, 0.1 mM EDTA, 10 mM $NaHCO_3$), and the tubes were supplemented with plant sterol esters (PSE) to make a total volume of 10 ml. Then, tubes were centrifuged, as described above, and the pellets were resuspended in 10 ml of PBS and maintained in ice.

Flow cytometry analysis. Single-cell suspensions from the lungs were seeded (10^6/well) in 96-well plates ("U" bottom), stained with allophycocyanin (APC)-conjugated CD45.2 (Biolegend, San Diego, CA, USA), phicoerithrin (PE)-conjugated CD11b (eBioscience San Diego, CA, USA), phicoerithrin cyanin 7 (PE Cy7)-conjugated Gr-1 (BD Bioscience, San Jose, CA, USA), peridinin chlorophyll 5.5 (PerCP Cy 5.5)-conjugated Ly6C and fluorescein isothiocyanate (FITC)-conjugated Ly6G antibodies (Biolegend) at a dilution 1:100 in PSE, and then incubated for 25 min at 4 °C, protected from light. After washing with PBS, the plate was centrifuged at 1500 rpm for 5 min at 4 °C. The pellets were resuspended in PBS, and immediately the plate was submitted to a BD Accuri C6 flow cytometer (BD Bioscience) to acquire 100,000 events in medium flow. The data were analyzed using FlowJo V10 Software (Three Star Inc., Ashland, OR, USA). Gating strategy for flow cytometry was followed to quantify $CD11b^+Gr\text{-}1^+$ (R2), $CD11b^+Ly6C^{high}Ly6G^-$/Monocytic (R4) and $CD11b^+$ $Ly6C^{low}$ $Ly6G^+$ /Granulocytic (R5) cells (Fig. 1).

Isolation of Gr-1$^+$ cells. Gr-1-positive cells were isolated using mouse Ly6G and Ly6C antibodies (BD Bioscience) and a BD Imagnet™ Cell Separation Magnet (BD Bioscience) following the manufacturer's instructions. $Gr\text{-}1^+$ cells were labelled with CD11b and Gr-1 antibodies, as described before. The purity of $Gr\text{-}1^+$ populations was > 95%, as determined by flow cytometry. Giemsa staining of 10^4 $Gr\text{-}1^+$ cells was performed to assess the polymorphonuclear and mononuclear morphology.

NO production. $Gr\text{-}1^+$ cells (10^6/well) were seeded in 24-well plates containing 1 ml of RPMI 10% SFB medium in the presence of LPS (Sigma-Aldrich, St Louis, MO, USA) at 1 µg/ml and incubated in a humid chamber at 37 °C for 18 h. After incubation, the medium was collected and centrifuged at 1500 rpm for 5 min. The supernatant was added to 96-well plates to measure nitrite content using a colorimetric Nitrite/Nitrate assay kit (Cayman Chemical Company, Ann Arbor, MI, USA), following the manufacturer's instructions. The absorbance at 540 nm was measured using a Multiskan X microplate plate reader.

Arginase assay. $Gr\text{-}1^+$ cells (10^6) were resuspended in 60 µl lysis buffer containing EDTA at 0.1 mM, Tris HCl at 50 mM (pH 7.5) and protease inhibitors (Sigma-Aldrich) and then lysed by freeze-and-thaw

cycles. The activity of arginase was determined from the urea production using the method described by Corraliza *et al*. [24]. The urea concentration was determined spectrophotometrically according to the absorbance at 550 nm measured using a Multiskan X microplate plate reader. The rate of urea production was used as an index for arginase activity.

The measurement of proteins for each sample (10 µl) was performed using a Nanodrop 2000 spectrophotometer (Thermo Fisher Scientific, Carlsbad, CA, USA), and then the ratio between of urea production to protein concentration was calculated (µM urea/µg protein).

ROS production. Oxidation-sensitive dye DCFDA was used to measure ROS production. Gr-1$^+$ cells (10^6) were labeled with 2.5 µM of CH-H_2DCFDA (5-(and-6)-chloromethyl-2',7'-dichlorodihydrofluorescein diacetate, acetyl ester) (Thermo Fisher Scientific), following the manufacturer's instructions. Next, cells were stained with APC CD45.2, PE CD11b, PE Cy7 Gr-1 PE antibodies, washed and centrifuged, as described before. The intensity of fluorescence was measured by flow cytometry and the data were expressed as median fluorescence intensity.

Statistical analysis. The data were analyzed and are expressed as the mean ± standard error (SE). Statistical analyses for single comparisons of mean values were performed using Student's *t*-test, and multiple comparisons were performed using ANOVA followed by Bonferroni's test in Graph pad prism version 5.0 (Graph pad Software, San Diego, CA, USA), http://www.graphpad.com. The value of Probability (p) lower than 0.05 was considered statistically significant.

RESULTS

At the end of the experiment, ES plasma levels of normal group and experimental groups were measured. Normal group showed 119.3 ± 3.43 µg/ml, control group 215.02 ± 7.46 µg/ml and ES group 302.4 ± 9.21 µg/ml. ES group had an increase of 2.53-fold the normal group (normal *vs* ES $p < 0.001$) and 1.40-fold compared to control (control *vs* ES $p < 0.001$). ES circulating levels corroborated our previous data [23].

ES gene therapy promoted a reduction in metastatic lesions and intratumoral CD11b$^+$Gr-1$^+$ cells. The CD11b$^+$Gr-1$^+$ cells and their subsets were assessed from metastatic lungs (Fig. 2). Initially, lung tissue sections were counted for the number of metastatic lesions. The number of metastatic lesions in the lung parenchyma of the control group was 80 ± 8, whereas the ES-treated group exhibited a significant reduction to 30.0 ± 4.3 ($p < 0.01$) (Fig. 2, *b*).

The accumulation of CD11b$^+$Gr-1$^+$ cells on the metastatic lungs after ES treatment. Our data showed that the control group exhibited a 1.9-fold increase in the percentage of CD11b$^+$Gr-1$^+$ cells compared to the normal group. In contrast, ES-treated group

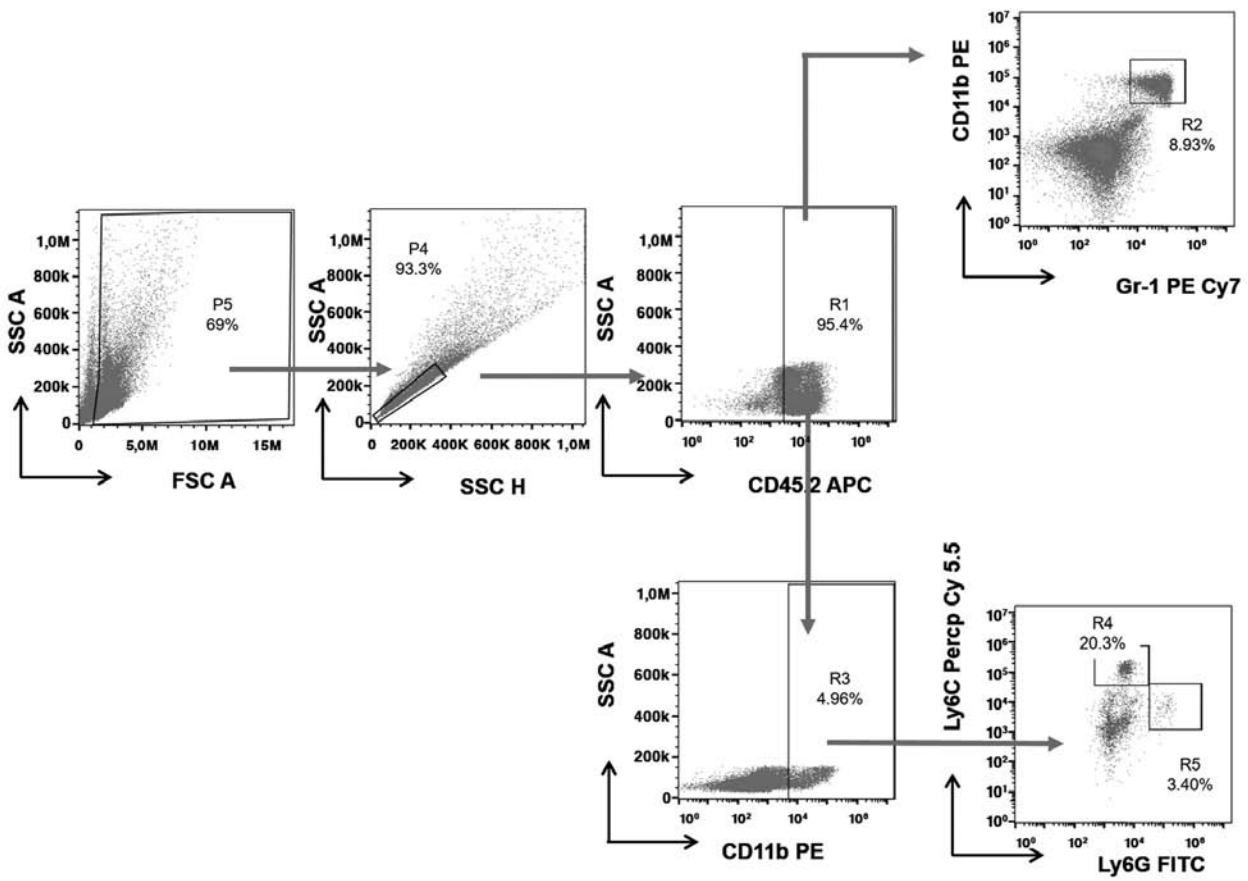

Fig. 1. Gating strategy for flow cytometry analysis. In this sample gating, cells were first gated on granularity and size by SSC-A *vs* FSC-A (P5), homogenous population for singlets by SSC-A *vs* SSC-H (P4), positive cells for CD45 (R1) and positive double for CD11b and Gr-1 (R2) for analysis of CD11b$^+$Gr-1$^+$ cells. To evaluate the monocytic and granulocytic cells, CD11b$^+$ cells were gated (R3) and finally these populations were measured in CD11b$^+$Ly6C^{high}Ly6G$^-$ (R4) and CD11b$^+$ Ly6C^{low}Ly6G$^+$ (R5) cells, respectively

exhibited a 3.8-fold decrease in $CD11b^+Gr\text{-}1^+$ cells compared to the control group ($p < 0.05$) (Fig. 2, *e*).

ES impaired preferentially intratumoral granulocytic cells and decreased G-CSF plasma levels (Fig. 3). Monocytic cells population did not change in the lungs of ES-treated group (Fig. 3, *b*). On the other hand, granulocytic cells were more predominant in healthy lungs and were significantly reduced by 39% and 75.4% in the control ($p < 0.01$) and ES ($p < 0.001$) groups, respectively, compared to the normal group (Fig. 3, *c*). However, our data showed a significant difference of 9.1% in the number of granulocytic cells between the control and ES groups ($p < 0.001$).

To assess whether ES treatment interfered with cytokine and soluble factor plasma levels related to the prevalence of granulocytic cells, we measured the levels of granulocytes-colony stimulating factor (G-CSF) using the Milliplex. The control group was 12.1-fold higher than the normal group ($p < 0.001$), whereas treatment with ES reduced the levels by 2.9-fold compared to the control group the G-CSF levels ($p < 0.05$) (Fig. 3, *d*).

$Gr\text{-}1^+$ cells purification and in vitro analysis. Previously, $Gr\text{-}1^+$ cells were magnetically isolated from metastatic tumors of the lungs, stimulated with LPS (1 μg/ml), and the nitrite and cellular arginase activities were determined. Therefore, ROS-producing $CD11b^+Gr\text{-}1^+$ cells were quantified via flow cytometry. The purity of the $Gr\text{-}1^+$ cells was approximately 97% (Fig. 4, *a*). Our data showed similar levels of nitrite in both the control and ES groups and undetected levels in the normal group (Fig. 4, *b*). On the other hand, arginase activity was reduced by 1.6-fold in the

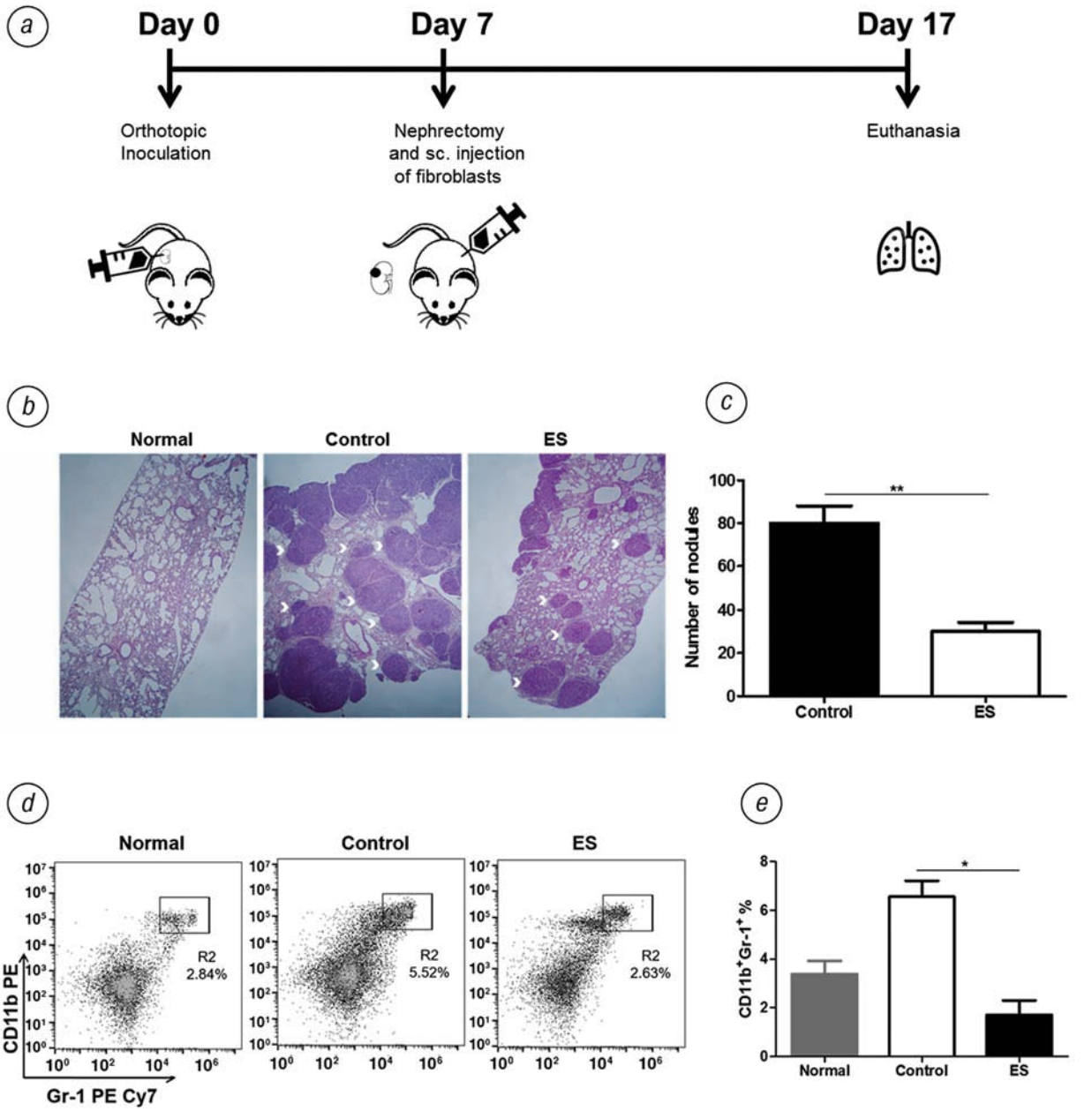

Fig. 2. Histopathological analysis of lung tissue sections by HE staining. Images captured observed in light microscopy at a 4× magnification: *a* — experimental design; *b* — graphs expressing number of nodules mean counted in lung tissue from control and ES-treated groups; *d* — quantification of $CD11b^+Gr\text{-}1^+$ cells (R2) in the metastatic lung after ES-treatment, representative dot plots (*c*) and graph expressing $CD11b^+Gr\text{-}1^+$ cells mean ± SEM; *e* — statistical analysis by Student's test considering $^*p < 0.05$ and $^{**}p < 0.01$

ES-treated group compared to the control group ($p = 0.56$) (Fig. 4, *c*). In contrast, ROS production was significantly reduced by 1.8-fold (Fig. 4, *e*).

DISCUSSION

Bone marrow-derived cells play important roles in tumor development. There are two major methods of vascular formation via vasculogenesis that involve endothelial progenitors and host inflammatory cells, such as macrophages and MDSC, which infiltrate tumor tissues, alter the microenvironment, and promote tumor angiogenesis [14, 25–28]. Our data demonstrated that kidneys containing tumors were able to recruit and accumulate intratumoral $CD11b^+Gr\text{-}1^+$ cells more than normal kidneys. This phenomenon has been demonstrated in patients with mRCC and could be explained by the production of soluble factors, such as VEGF, cytokines and proinflammatory substances [12, 15, 29–31]. Here, we detected monocytic cells into the tumor microenvironment, which supports the hypothesis that this subtype is able to tolerate hypoxic and acidic environments [32].

The tumor microenvironment is able to partially block the differentiation of IMC and, consequently, promote the expansion of immature cells in the bone marrow [10, 12, 15, 33, 34]. The data presented in this study demonstrated that $CD11b^+Gr\text{-}1^+$ cells, particularly the granulocytic subtype, were expanded

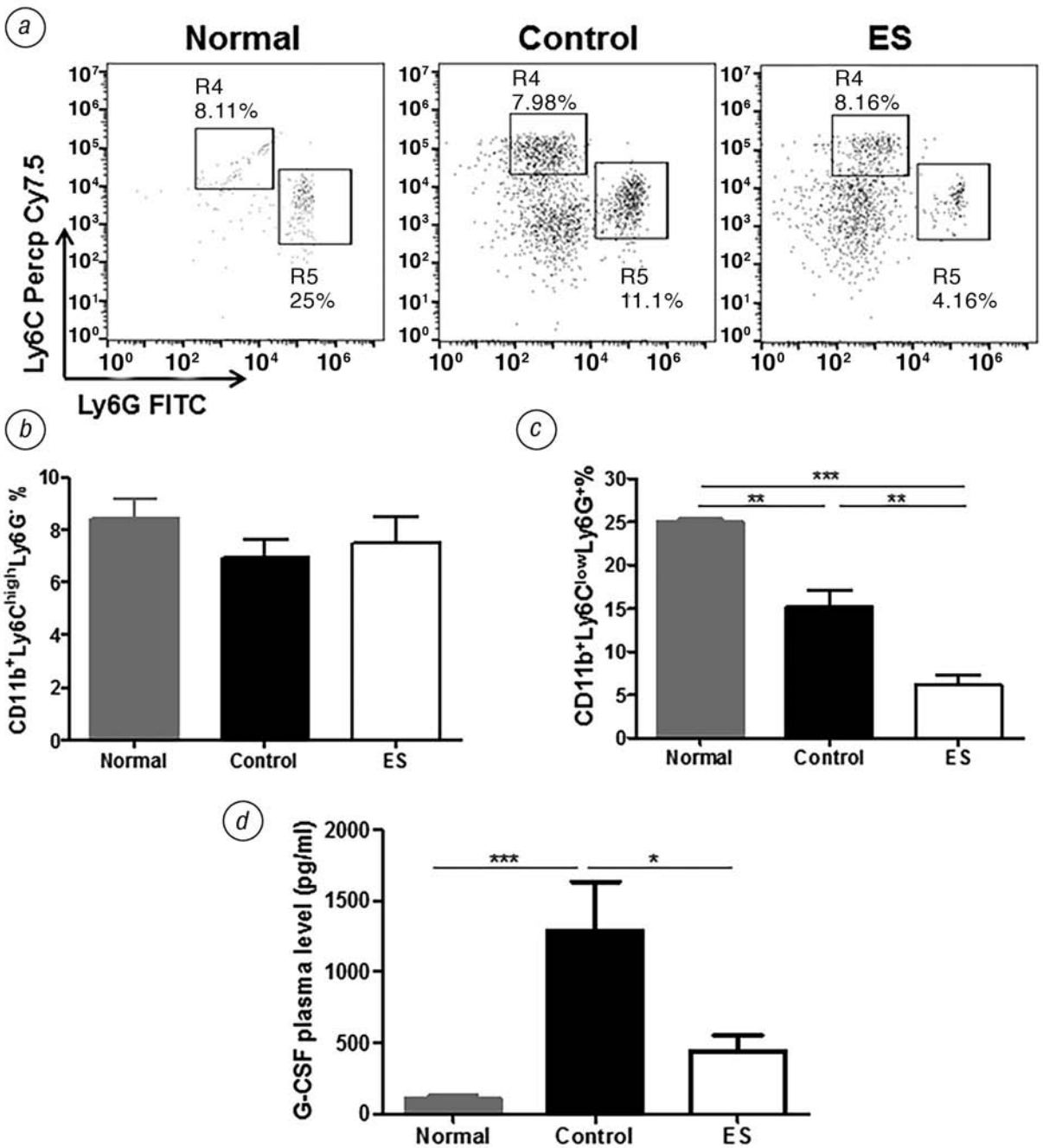

Fig. 3. Quantification of monocytic (R4) and granulocytic (R5) cells in lung after treatment with ES. Representative dot plots, (*a*) graph expressing monocytic cells (R4) (*b*) and granulocytic cells (R5) mean. (*c*) Determination of plasma levels of soluble factor and cytokine measured by Milliplex. G-CSF (*d*) levels were determined in the plasma from normal, control and ES-treated groups. Statistical analysis by ANOVA followed by Bonferroni's test considering $*p < 0.05$, $**p < 0.01$ and $***p < 0.001$

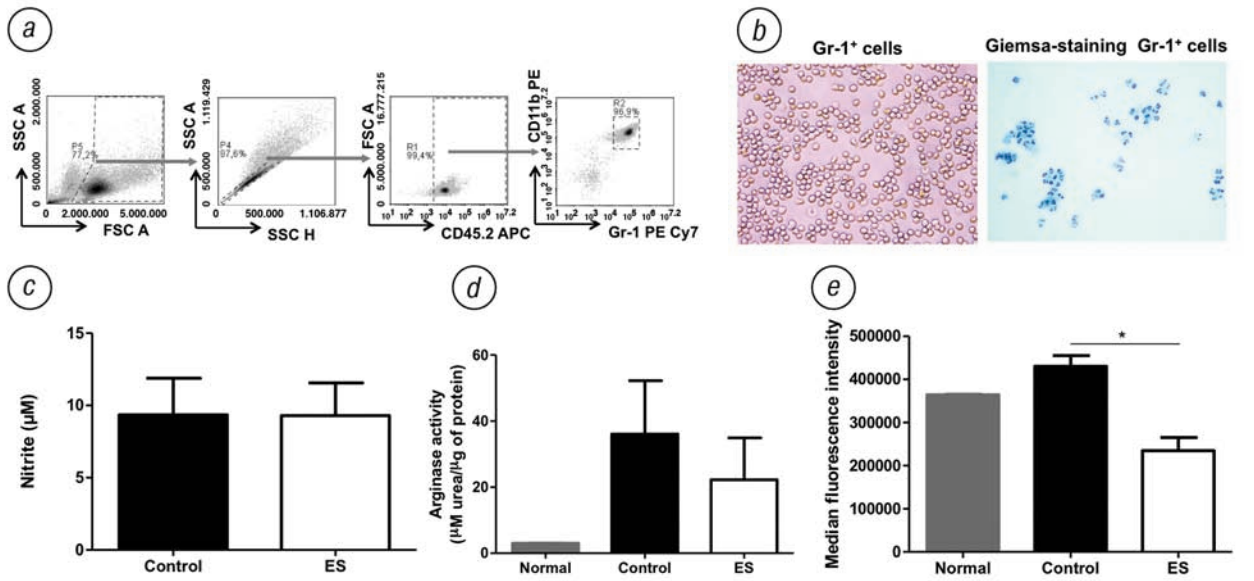

Fig. 4. Functional analysis of magnetically Gr-1$^+$ cells separated of lungs from normal, control and ES-treated groups. Dot plots showing strategy gating of delimited cells by SSC *vs* FSC (P5), homogenous population by SSC-A *vs* SSC-H (P4), CD45$^+$ cells (R1) and positive double for CD11b and Gr-1 (R2) to evaluate the purity of Gr-1$^+$ cells (*a*). Gr-1$^+$ cells visualized *in vitro* and Giemsa staining showed these cells to have polymorphonuclear and monuclear morphologies (400× magnification) (*b*). Measurement of nitrite produced by LPS-stimulated Gr-1$^+$ cells obtained of lungs (*c*). The cellular arginase activity of Gr-1$^+$ cells stimulated with LPS for 18 h (*d*) and median fluorescence intensity of the ROS production. (*e*) Statistical analysis by Student's *t*-test and ANOVA followed by Bonferroni's test considering. $*p < 0.05$

in bone marrow, which corroborates data reported in the literature [35–37]. The lymphoid organ is described as a locale where PMN-MDSC cells mediate the antigen-specific suppressive mechanisms [12]. Our findings showed that the accumulation of splenic CD11b$^+$Gr-1$^+$ cells is directly associated with metastatic progression of, preferentially, the granulocytic subtype on days 14 and 17.

Several pro-tumorigenic activities have been associated with the involvement of CD11b$^+$Gr-1$^+$ myeloid cells in the metastatic process, including the expression of proangiogenic factor Bv8, metastasis-promoting lysil oxidase MMP-9 secretion, TGF-β-mediated metastasis and immune tolerance and suppression by virtue of MDSC activity [14, 38, 39]. Here, we identified that the accumulation of CD11b$^+$Gr-1$^+$ cells in metastatic lungs was inversely proportional to the metastatic process. Studies have revealed that CD11b$^+$Gr-1$^+$ cells change the pre-metastatic lung into an inflammatory and proliferative environment, promoting macrometastasis [39, 40]. In addition, advanced metastatic progression showed different sizes of metastatic lesions.

One of the most critical challenges in cancer treatment is the absence of a functional immune system capable of efficiently controlling tumor development. However, most chemotherapeutic agents and radiation therapy also suppress the immune system. A selective panel of anticancer agents have been reported for their ability to selectively target immunosuppressive cells, such as Treg and MDSC, thereby enhancing the efficacy of immunotherapy [15, 41, 42].

Accordingly, we previously demonstrated that ES gene therapy elicits a pleotropic effect in the mRCC model, primarily as a potent pro-inflammatory and antitumor response, as observed on day 17 [43, 44]. The production of ES by fibroblasts was 2.5-fold higher than that of non-producing fibroblasts, and the administration of these cells promoted a reduction in the metastatic foci number, corroborating our previous data [45].

Based on these findings, we hypothesize that ES gene therapy may also have the potential to reduce the number of CD11b$^+$Gr-1$^+$ cells, selectively targeting the granulocytic subtype. In addition, this effect was associated with a significant reduction in the level of circulating G-CSF. Additionally, high G-CSF levels have been reported in several tumor models and have been associated with increased expansion and recruitment of granulocytic cells, inducing proangiogenic and immunosuppressive activities [46, 47]. However, cytokines present in the tumor microenvironment, such as IL-1β, were reduced after treatment with ES, suggesting an important role in myelopoiesis by generating MDSC [48]. These findings are contrary to those reported by Zhang et al. [49].

According to these observations, we analyzed the *in vitro* Gr-1$^+$ cells obtained from the experimental groups and observed that the ES-treated group exhibited reduced arginase activity and reduced production of ROS associated with the antigen-specific immunosuppressive mechanism used by granulocytic cells.

In this study, we provide, for the first time, the profile of CD11b$^+$Gr-1$^+$ cells in an orthotopic mRCC animal model and the effect of antiangiogenic gene therapy on these cells and their function. This report indicates that treatment with ES can be effective in modulating soluble factors for suppressing in the number of granulocytic cells and their function. Hence, our study highlights the use of ES as a regulator of the im-

munosuppressive response and as a promising target for use in combined therapies.

ACKNOWLEDGEMENTS

This study was supported by FAPESP (process: 2012/12955-2).

CONFLICT OF INTERESTS

The authors declare no competing financial interest.

REFERENCES

1. American Cancer Society. What are the key statistics about kidney cancer? Atlanta, Ga: American Cancer Society; 2016.

2. Scelo G, Hofmann JN, Banks RE, ***et al.*** International cancer seminars — a focus on kidney cancer. Ann Oncol 2016; **27**: 1382–5.

3. Protzel C, Maruschke M, Hakenberg OW. Epidemiology, aetiology, and pathogenesis of renal cell carcinoma. Eur Associat Urol 2012; **11**: 52–9.

4. Grivas N, Kafarakis V, Tsimaris I, ***et al.*** Clinico-pathological prognostic factors of renal cell carcinoma: A 15-year review from a single center in Greece. Urol Ann 2014; **6**: 116–21.

5. Muglia VF, Prando A. Carcinoma de células renais: classificação histológica e correlação com métodos de imagem. Radiol Brasileira 2015; **48**: 166–74.

6. Motzer RJ, Escudier B, Oudard S, ***et al***. Efficacy of everolimus in advanced renal cell carcinoma: a double-blind, randomised, placebo-controlled phase III trial. Lancet 2008; **372**: 449–56.

7. Verine J, Pluvinage A, Bousquet G, ***et al***. Hereditary renal cancer syndromes: an update of a systematic review. Eur Urol 2010; **58**: 701–10.

8. Cowey CL, Hutson TE. Molecularly targeted agents for renal cell carcinoma: the next generation. Clin Adv Hematol Oncol 2010; **8**: 357–60.

9. Dvorak HF, Weaver VM, Tlsty TD, Bergers G. Tumor microenvironment and progression. J Surg Oncol 2011; **103**: 468–74.

10. Ostrand-Rosenberg S. Myeloid-derived suppressor cells: more mechanisms for inhibiting antitumor immunity. Cancer Immunol Immunother 2010; **59**: 1593–600.

11. Sevko A, Umansky VV. Myeloid-derived suppressor cells interact with tumors in terms of myelopoiesis, tumorigenesis and immunosuppression: thick as thieves. J Cancer 2013; **4**: 3–11.

12. Gabrilovich DI, Nagaraj S. Myeloid-derived suppressor cells as regulators of the immune system. Nat Rev Immunol 2009; **9**: 162–74.

13. Greten TF, Manns MP, Korangy F. Myeloid-derived suppressor cells in human diseases. Int Immunopharmacol 2011; **11**: 802–7.

14. Condamine T, Gabrilovich DI. Molecular mechanisms regulating myeloid-derived suppressor cell differentiation and function. Trends Immunol 2011; **32**: 19–25.

15. Nagaraj S, Gupta K, Pisarev V, ***et al.*** Altered recognition of antigen is a novel mechanism of CD8+ T cell tolerance in cancer. Nat Med 2007; **13**: 828–35.

16. Mazzoni A, Bronte V, Visintin A, ***et al.*** Myeloid suppressor lines inhibit T cell responses by an NO dependent mechanism. J Immunol 2002; **168**: 689–95.

17. O'Reilly MS, Boehm T, Shing Y, ***et al.*** Endostatin: an endogenous inhibitor of angiogenesis and tumor growth. Cell 1997; **88**: 277–85.

18. Rehn M, Veikkola T, Kukk-Valdre E, ***et al***. Interaction of endostatin with integrins implicated in angiogenesis. Proc Natl Acad Sci 2001; **98**: 1024–9.

19. Abdollahi A, Hahnfeldt P, Maercker C. Endostatin's antiangiogenic signaling network. Mol Cell 2004; **13**: 649–63.

20. Ren Z, Wang Y, Jiang W, ***et al***. Anti-tumor effect of a novel soluble recombinant human endostatin: administered as a single agent or in combination with chemotherapy agents in mouse tumor models. PLoS One 2014; **9**: e107823.

21. Ozao-Choy J, Ma G, Kao J, ***et al.*** The novel role of tyrosine kinase inhibitor in the reversal of immune suppression and modulation of tumormicroenvironment for immune-based cancer therapies. Cancer Res 2009; **69**: 2514–22.

22. Farsaci B, Donahue N, Coplin MA, ***et al***. Immune consequences of decreasing tumor vasculature with anti-angiogenic tyrosine kinase inhibitors in combination with therapeutic vaccines. Cancer Immunol Res 2014; **2**: 1090–102.

23. Rocha FGG, Chaves KCB, Chammas R, ***et al***. Endostatin gene therapy enhances the efficacy of IL-2 in suppressing metastatic renal cell carcinoma in mice. Cancer Immunol Immunother 2010; **59**: 1357–65.

24. Corraliza IM, Campo ML, Soler G, Modolell M. Determination of arginase activity in macrophages: a micromethod. J Immunol Methods 1994; **174**: 231–5.

25. Asahara T, Murohara T, Sullivan A, ***et al***. Isolation of putative progenitor endotelial cells for angiogenesis. Science 1997; **275**: 964–7.

26. Carmeliet P, Moons L, Luttun A, ***et al***. Synergism between vascular endotelial growth factor and placental growth factor contributes to angiogenesis and plasma extravasation in pathological conditions. Nat Med 2007; **7**: 575–83.

27. Lyden D, Hattori K, Dias S, ***et al***. Impaired recruitment of bone-marrow-derived endotelial and hematopoietic precursor cells blocks tumor angiogenesis and growth. Nat Med 2001; **7**: 1194–201.

28. Kamate C, Baloul S, Grootenboer S, ***et al***. Inflammation and cancer, the mastocytoma P815 tumor model revisited: triggering of macrophage activation *in vivo* with pro-tumorigenic consequences. Int J Cancer 2002; **100**: 571–9.

29. Kusmartsev S, Eruslanov E, Kubler H, ***et al.*** Oxidative stress regulates expression of VEGFR1 in myeloid cells: link to tumor-induced immune suppression in renal cell carcinoma. J Immunol 2008; **181**: 346–53.

30. Finke J, Ko J, Rini B, ***et al***. MDSC as a mechanism of tumor escape from Sunitinib mediated anti-angiogenic therapy. Int Immunopharmacol 2011; **11**: 853–8.

31. Ko J, Rayman P, Ireland J, ***et al.*** Direct and differential suppression of myeloid-derived suppressor cell subsets by Sunitinib is compartmentally constrained. Cancer Res 2010; **70**: 3526–36.

32. Youn J, Gabrilovich DI. The biology of myeloid-derived suppressor cells: The blessing and the curse of morphological and functional heterogeneity. Eur J Immunol 2010; **40**: 2969–75.

33. Ribechini E, Greifenberg V, Sandwick S, Lutz MB. Subsets, expansion and activation of myeloid-derived suppressor cells. Med Microbiol Immunol 2010; **199**: 273–81.

34. Dolcetti L, Marigo L, Mantelli B, ***et al***. Myeloid-derived suppressor cell role in tumor-related inflammation. Cancer Lett 2008; **267**: 216–25.

35. Teixeira D, Almeida JS, Visniauskas B, ***et al***. Myeloid-derived suppressor cells and associated events in urethane-induced lung cancer. Clinics 2013; **68**: 858–64.

36. Youn J, Collazo M, Shalova IN, ***et al***. Characterization of the nature of granulocytic myeloid-derived suppressor cells in tumor-bearing mice. J Leukocyte Biol 2012; **91**: 167–74.

37. Gabrilovich DI, Ostrand-Rosenberg S, Bronte V. Coordinated regulation of myeloid cells by tumours. Nat Ver Immunol 2013; **12**: 253–68.

38. Erler JT, Bennewith KL, Cox TR, ***et al***. Hypoxia-induced lysyl oxidase is a critical mediator of bone marrow cell recruitment to form the pre-metastatic niche. Cancer Cell 2009; **15**: 35–44.

39. Yan HH, Pickup M, Pang Y. Gr-1+CD11b+ myeloid cells tip the balance of immune protection to tumor promotion in the premetastatic lung. Cancer Res 2010; **70**: 6139–49.

40. Gao D, Vahdat LT, Wong S. Microenvironmental regulation of epithelial-mesenchymal transitions in cancer. Cancer Res 2012; **72**: 4883–9.

41. Wesolowski R, Markowitz J, Carson WE. Myeloid-derived suppressor cells — a new therapeutic target in the treatment of cancer. J Immunother Cancer 2013; **1**: 1–11.

42. Alizadeh D, Trad M, Hanke NT, ***et al***. Doxorubicin eliminates myeloid-derived suppressor cells and enhances the efficacy of adoptive T-cell transfer in breast cancer. Cancer Res 2014; **74**: 104–18.

43. Chaves KCB, Peron JPS, Chammas R, ***et al.*** Endostatin gene therapy stimulates upregularion of ICAM-1 and VCAM-1 in a metastatic renal cell carcinoma model. Cancer Gene Therapy 2012; **19**: 558–65.

44. Foguer K, Braga SM, Peron SPJ***, et al***. Endostatin gene therapy inhibits intratumoral macrophage M2 polarization. Biomed Pharmacother 2016; **79**: 102–11.

45. Braga SM, Foguer K, Chaves KCB, ***et al***. Involvement of NF-kbp50/Bcl-3 complex in response to antiangiogenic therapy in mouse model of metastatic renal cell carcinoma. Biomed Pharmacother 2014; **68**: 873–9.

46. Waight JD, Hu Q, Miller A, ***et al***. Tumor-derived G-CSF facilitates neoplastic growth through a granulocytic myeloid-derived suppressor cell-dependent mechanism. PloS One 2011; **6**: 27690.

47. Kowanetz M, Wu X, Lee J, ***et al.*** Granulocyte-colony stimulating factor promotes lung metastasis through mobilization of Ly6G+Ly6C+ granulocytes. PNAS 2010; **107**: 21248–55.

48. Elkabets M, Ribeiro VS, Dinarello CA. IL-1β regulates a novel myeloid-derived suppressor cell subset that impairs NK cell development and function. Eur J Immunol 2010; **40**: 3347–57.